CrystEngComm

High-Pressure Crystallographic and Spectroscopic Studies on Two Molecular Dithienylethene Switches

Christopher H Woodall, Simon K. Brayshaw, Stefanie S. Schiffers, Paul R. Raithby, Dave R. Allan, Simon Parsons, Rafael Valiente

CONTENTS

Synthetic details

All synthetic procedures involving the handling and preparation of air water sensitive reagents were performed using standard Schlenk techniques under an atmosphere of purified nitrogen. All solvents involved in the handling of air or water sensitive species were dried prior to use using an automated solvent purification system. All chemicals were purchased from a commercial source and used without further purification unless stated. NMR spectroscopy was performed at room temperature on one of the following instruments; a Bruker Avance 300 MHz Ultrashield NMR spectrometer; a Bruker Avance 400 MHz NMR spectrometer or Bruker Avance 500 MHz NMR spectrometer. All spectra were collected in deuterated chloroform unless otherwise stated. single Room temperature crystal X-ray diffraction experiments was performed on an Oxford Diffraction Gemini A Ultra diffractometer at the University of Bath equipped with an Oxford Instruments Cryojet XL crystal cooling device in order to determine crystal suitability for high pressure experiments.

Table 1. Full crystallographic parameters for 1,2-Bis(2-methyl benzothiophen-3-yl)perfluorocyclopentene

Pressure (GPa)	**ambient**	**0.86**	**2.09**	**2.55**	**3.38**	**4.08**	**4.45**	**5.38**	**5.50**
Formula	$C_{23}H_{14}F_6S_2$	$C_{23}H_{14}F_6S_2$	$C_{23}H_{14}F_6S_2$	$C_{23}H_{14}F_6S_2$	$C_{23}H_{14}F_6S_2$	$C_{23}H_{14}F_6S_2$	$C_{23}H_{14}F_6S_2$	$C_{23}H_{14}F_6S_2$	$C_{23}H_{14}F_6S_2$
M_r	468.46	468.46	468.46	468.46	468.46	468.46	468.46	468.46	468.46
Crystal System	Monoclinic	Monoclinic	Monoclinic	Monoclinic	Monoclinic	Monoclinic	Monoclinic	Monoclinic	Monoclinic
Space Group	$P2_1/n$	$P2_1/n$	$P2_1/n$	$P2_1/n$	$P2_1/n$	$P2_1/n$	$P2_1/n$	$P2_1/n$	$P2_1/n$
a,b,c (Å)	11.4349(6) 15.5450(6) 12.8179(6)	11.262(6) 14.9356(12) 12.497(4)	11.096(2) 14.494(3) 12.262(3)	11.053(2) 14.338(3) 12.136(2)	10.991(6) 14.1391(8) 12.033(4)	10.954(2) 14.032(3) 11.962(2)	10.930(2) 13.961(3) 11.922(2)	10.135(9) 15.0384(16) 10.900(7)	10.118(18) 15.012(3) 10.877(11)
β (°)	113.755(6)	113.73(6)	113.85(3)	113.76(3)	113.83(5)	113.77(3)	113.76(3)	107.52(9)	107.53(16)
V (Å^3)	2085.41(17)	1924.3(13)	1803.7(6)	1760.4(6)	1710.6(10)	1682.7(6)	1665.0(6)	1584.3(17)	1575(3)
Z/Z'	4/1	4/1	4/1	4/1	4/1	4/1	4/1	4/1	4/1
D_x (Mg m^{-3})	1.492	1.617	1.725	1.768	1.819	1.849	1.869	1.964	1.975
μ(mm^{-1})	0.316	0.264	0.282	0.289	0.297	0.302	0.305	0.321	0.323
F(000)	952	952	952	952	952	952	952	952	952
2θ range(°)	3.09/29.29	3.33/25.55	3.35/22.53	3.38/23.97	3.32/25.52	3.34/22.42	3.36/22.63	3.33/25.55	3.33/25.57
R_{int}	0.0266	0.0846	0.0789	0.1017	0.0769	0.0515	0.0635	0.0679	0.0780
Completeness	0.999	0.327	0.359	0.323	0.319	0.363	0.367	0.321	0.305
No. Measured/ Independent Observed reflections	27119/5221	6487/1294	4474/933	4747/976	5749/1116	4815/873	4932/891	5277/1046	5291/992
R[F]/wR[F2] (for I >2σ) **R[F]/wR[F2] (all data)**	0.0571/0.1517 0.0797/0.1693	0.0989/0.2333 0.1415/0.2625	0.0775/0.1535 0.1037/ 0.1713	0.0770/0.1592 0.1241/0.1864	0.0758/0.1681 0.0974/0.1797	0.0674/0.1630 0.0753/0.1687	0.0687/0.1658 0.0797/0.1730	0.0561/0.1083 0.0794/0.1193	0.0545/0.1129 0.0724/0.1223
Restraints/Parameters	0/282	70/137	68/137	68/137	68/137	68/137	68/137	68/137	69/137
$\Delta\rho_{max},\Delta\rho_{min}$ (e Å^{-3})	0.851/-0.406	0.463/-0.427	0.363/-0.376	0.397/-0.363	0.423/-0.347	0.379/-0.303	0.459/-0.315	0.351/-0.320	0.346/-0.351

Table 1(cont.). Full crystallographic parameters for 1,2-Bis(2-methyl benzothiophen-3-yl)perfluorocyclopentene

Pressure (GPa)	**5.60**	**6.56**	**7.40**	**8.90**
Formula	$C_{23}H_{14}F_6S_2$	$C_{23}H_{14}F_6S_2$	$C_{23}H_{14}F_6S_2$	$C_{23}H_{14}F_6S_2$
M_r	468.46	468.46	468.46	468.46
Crystal System	Monoclinic	Monoclinic	Monoclinic	Monoclinic
Space Group	$P2_1/n$	$P2_1/n$	$P2_1/n$	$P2_1/n$
a,b,c (Å)	10.117(18) 15.004(3) 10.869(11)	10.052(2) 14.932(3) 10.789(2)	9.985(2) 14.855(3) 10.722(2)	9.894(2) 14.736(3) 10.588(2)
β (°)	107.52(16)	107.39(3)	107.35(3)	107.21(3)
V (Å^3)	1573(3)	1545.4(5)	1517.9(5)	1474.6(5)
Z/Z'	4/1	4/1	4/1	4/1
D_x (Mg m^{-3})	1.978	2.013	2.050	2.110
μ(mm^{-1})	0.323	0.329	0.335	0.345
F(000)	952	952	952	952
2θ range(°)	4.03/25.51	3.35/22.60	3.29/22.32	3.32/25.25
R_{int}	0.0671	0.0921	0.1450	0.0661
Completeness	0.298	0.357	0.334	0.309
No. Measured/ Independent Observed reflections	5013/961	4424/801	2902/711	4687
R[F]/wR[F2] (for I >2σ) **R[F]/wR[F2] (all data)**	0.0548/0.1277 0.0710/0.1354	0.0504/0.1042 0.0710/0.1170	0.0780/0.1827 0.1027/0.2080	0.0436/0.0962 0.0557/0.1031
Restraints/Parameters	68/137	68/137	68/137	68/137
$\Delta\rho_{max}$,$\Delta\rho_{min}$ (e Å^{-3})	0.380/-0.396	0.279/-0.283	0.311	0.350/-0.375

Table 2. Full crystallographic parameters for 1,2-Bis(2,5-dimethylthiophen-3-yl)perfluorocyclopentene

Pressure (GPa)	**ambient**	**0.71**	**1.02**	**2.52**	**3.64**	**4.15**	**5.70**	**6.70**	**7.40**
Formula	$C_{17}H_{14}F_6S_2$	$C_{17}H_{14}F_6S_2$	$C_{17}H_{14}F_6S_2$	$C_{17}H_{14}F_6S_2$	$C_{17}H_{14}F_6S_2$	$C_{17}H_{14}F_6S_2$	$C_{17}H_{14}F_6S_2$	$C_{17}H_{14}F_6S_2$	$C_{17}H_{14}F_6S_2$
M_r	396.42	396.42	396.42	396.42	396.42	396.42	396.42	396.42	396.42
Crystal System	Monoclinic	Monoclinic	Monoclinic	Monoclinic	Monoclinic	Monoclinic	Monoclinic	Monoclinic	Monoclinic
Space Group	*C2/c*	*C2/c*	*C2/c*	*C2/c*	*C2/c*	*C2/c*	*$P2_1/c$*	*$P2_1/c$*	*$P2_1/c$*
a,b,c (Å)	20.5687(10) 8.8331(2) 11.4381(5)	19.672(3) 8.6717(8) 11.0787(9)	19.325(6) 8.6243(7) 10.9544(7)	18.427(5) 8.4721(6) 10.6330(7)	18.050(11) 8.3848(8) 10.551(23)	17.874(8) 8.3360(8) 10.524(13)	10.506(2) 16.364(3) 15.514(3)	10.4886(10) 16.3135(16) 15.560(10)	10.4663(8) 16.2590(12) 15.4270(72)
β (°)	122.177(6)	120.594(13)	120.113(14)	118.512(15)	118.132(23)	117.9(2)	98.95(3)	99.081(16)	99.409(12)
V (Å^3)	1758.95(12)	1626.8(4)	1579.3(6)	1458.6(5)	1408.2(1)	1385.9(8)	2634.7(9)	2629.1(15)	2589.9(11)
Z/Z'	4/½	4/½	4/½	4/½	4/½	4/½	8/2	8/2	8/2
D_x (Mg m^{-3})	1.497	1.618	1.667	1.805	1.870	1.900	1.999	2.003	2.033
μ(mm^{-1})	0.359	0.304	0.313	0.339	0.351	0.357	0.375	0.376	0.382
F(000)	808	808	808	808	808	808	1616	808	808
2θ range(°)	2.91/32.97	4.34/25.83	4.44/25.93	4.53/25.95	2.66/28.06	4.50/25.50	4.50/25.50	3.45/25.62	3.47/25.63
R_{int}	0.0327	0.0903	0.0549	0.0578	0.0563	0.0851	0.0670	0.0971	0.0481
Completeness	0.996	0.253	0.275	0.266	0.254	0.299	0.281	0.282	0.290
No. Measured/ Independent Observed reflections	55042/3177	2588/434	2656/444	2070/398	1296/	1864/426	8389/1452	5726/1536	7408/1557
R[F]/wR[F2] (for I >2σ) **R[F]/wR[F2] (all data)**	0.0410/0.1143 0.0577/0.1293	0.0766/0.1825 0.0963/0.1996	0.0728/0.1772 0.0883/0.1906	0.0713/0.1441 0.0832/0.1505	0.0982/0.2321 0.1193/0.2507	0.0934/0.1927 0.1031/0.1994	0.0712/0.1779 0.0922/0.2025	0.0689/0.1714 0.0850/0.1851	0.0615/0.1650 0.0718/0.1752
Restraints/Parameters	28/154	28/74	28/74	28/74	28/74	28/74	85/229	85/224	85/229
$\Delta\rho_{max}$,$\Delta\rho_{min}$ (e Å^{-3})	0.300	0.360	0.436	0.399	0.482	0.512	0.559	0.463	0.497

Table 2(cont). Full crystallographic parameters for 1,2-Bis(2,5-dimethylthiophen-3-yl)perfluorocyclopentene

Pressure (GPa)	**8.55**	**9.50**	**9.80**
Formula	$C_{17}H_{14}F_6S_2$	$C_{17}H_{14}F_6S_2$	$C_{17}H_{14}F_6S_2$
M_r	396.42	396.42	396.42
Crystal System	Monoclinic	Monoclinic	Monoclinic
Space Group	*$P2_1/c$*	*$P2_1/c$*	*$P2_1/c$*
a,b,c (Å)	10.4211(7) 16.1206(12) 15.159(7)	10.377(2) 16.060(3) 15.031(3)	10.3834(5) 16.0279(8) 15.022(5)
β (°)	99.830(11)	100.44(3)	100.443(7)
V (Å^3)	2509.3(11)	2463.5(9)	2458.6(7)
Z/Z'	8/2	8/2	8/2
D_x (Mg m^{-3})	2.099	2.138	2.142
μ(mm^{-1})	0.394	0.401	0.402
F(000)	1616	1616	1616
2θ range(°)	3.51/25.68	3.26/25.25	3.54/25.58
R_{int}	0.1016	0.1037	0.0616
Completeness	0.258	0.277	0.269
No. Measured/ Independent Observed reflections	5197/1349	7068/1356	7870/1359
R[F]/wR[F2] (for I >2σ) **R[F]/wR[F2] (all data)**	0.0613/0.1546 0.0795/0.1699	0.0824/0.1875 0.1158/0.2172	0.0525/0.1281 0.0718/0.1458
Restraints/Parameters	85/229	85/209	85/209
$\Delta\rho_{max}$,$\Delta\rho_{min}$ (e Å^{-3})	0.404	0.463	0.468

Unit cell parameters for Compound 2

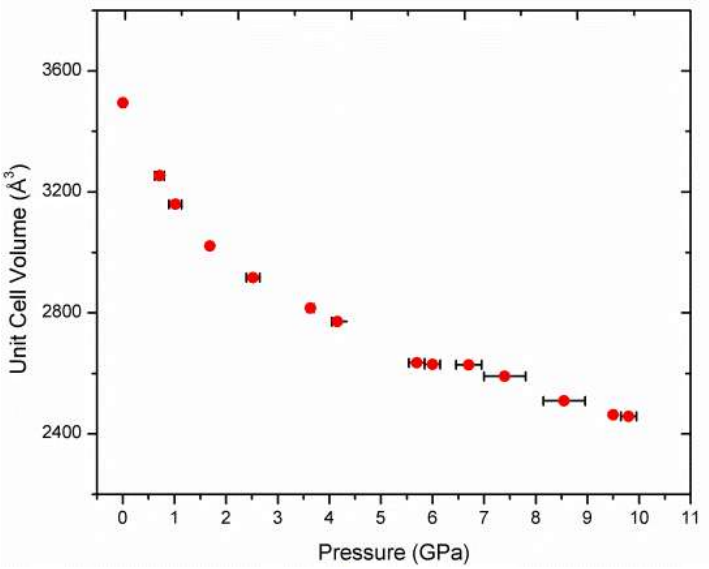

Figure 1. Unit cell volume of **2** with pressure.

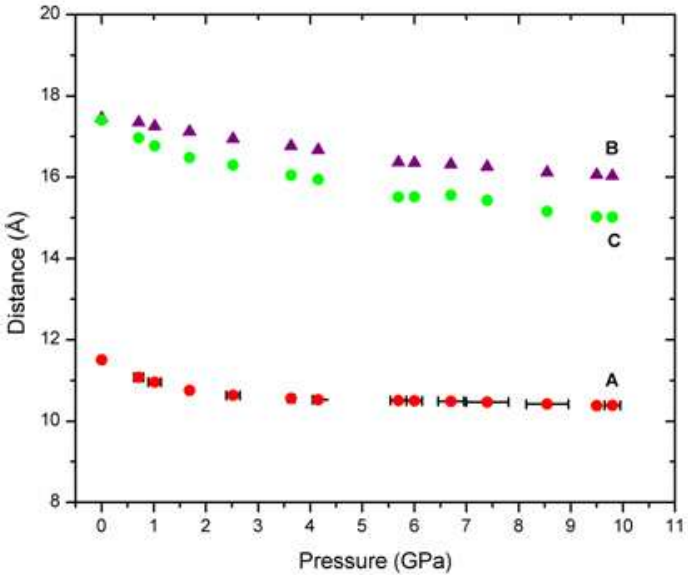

Figure 2. Unit cell parameters of **2** with pressure.

Equation of State

Table 3. Results of equation of state calculations from EOSFit for 1,2-Bis(2-methyl benzothiophen-3-yl)perfluorocyclopentene fitted to the data between 0.00 and 4.45 GPa.[1]

Equation fitted	Parameter					
	V_0	B_0	B’	B’’	X^2w	$delP_{max}$
Murnaghan	2085.40(5)	7.89(1.73)	7.00(1.82)	-	0.0363	0.143
Birch Murnaghan 2nd order	2085.43(5)	11.38(0.31)	“4”	-	0.7391	0.427
Birch Murnaghan 3rd order*	2085.44(5)	7.41(2.14)	9.2(4.2)	-4.86848	0.0512	0.172
Birch Murnaghan 4th order	2085.43(6)	9.29(6.05)	1.947(17.555)	5.86(7.16)	0.0317	0.146

*Third order Birch Murnaghan chosen for overall best fit.

Table 4. Results of equation of state calculations from EOSFit for 1,2-Bis(2,5-dimethylthiophen-3-yl)perfluorocyclopentene between 0.00 and 4.15 GPa .[1]

Equation fitted	Parameter					
	V_0	B_0	B’	B’’	X^2w	$delP_{max}$
Murnaghan *	1747.68(6)	6.14(3)	8.08(40)		06408	0.113
Birch Murnaghan 2nd order	1747.66(23)	9.95(52)	“4”		19.4382	0.479
Birch Murnaghan 3rd order	1747.69(2)	4.92(54)	14.31(2.23)	-24.51872	1.0108	0.149
Birch Murnaghan 4th order	1747.67(5)	8.77(2.44)	-0.043(4.98)	6.99(3.13)	0.4776	0.077

``

*Murnaghan chosen for overall best fit.

Detailed analysis of 1,2-Bis(2,5-dimethylthiophen-3-yl)perfluorocyclopentene

Under ambient conditions **2** crystallises in the space group *C2/c*. When the unit contents are analysed it is clear that there is only ½ a molecule in the asymmetric unit. The asymmetric unit in the unit cell sits on a two-fold rotation axis running parallel to the *b* axis relating two halves of the molecule as shown in the top image of Figure 3. Upon the phase transition at ~ 5 GPa, the two fold rotation axes disappear resulting in a doubling of the *b* axis, transforming the cell to $P2_1/c$, quadrupling the number of molecules in the asymmetric unit from ½ to 2 complete molecules, resulting in a doubling of unit cell volume. The new phase is a previously unreported phase of **2**. It is apparent that there are several changes in the new phase when compared to the ambient phase and other lower temperature phases.

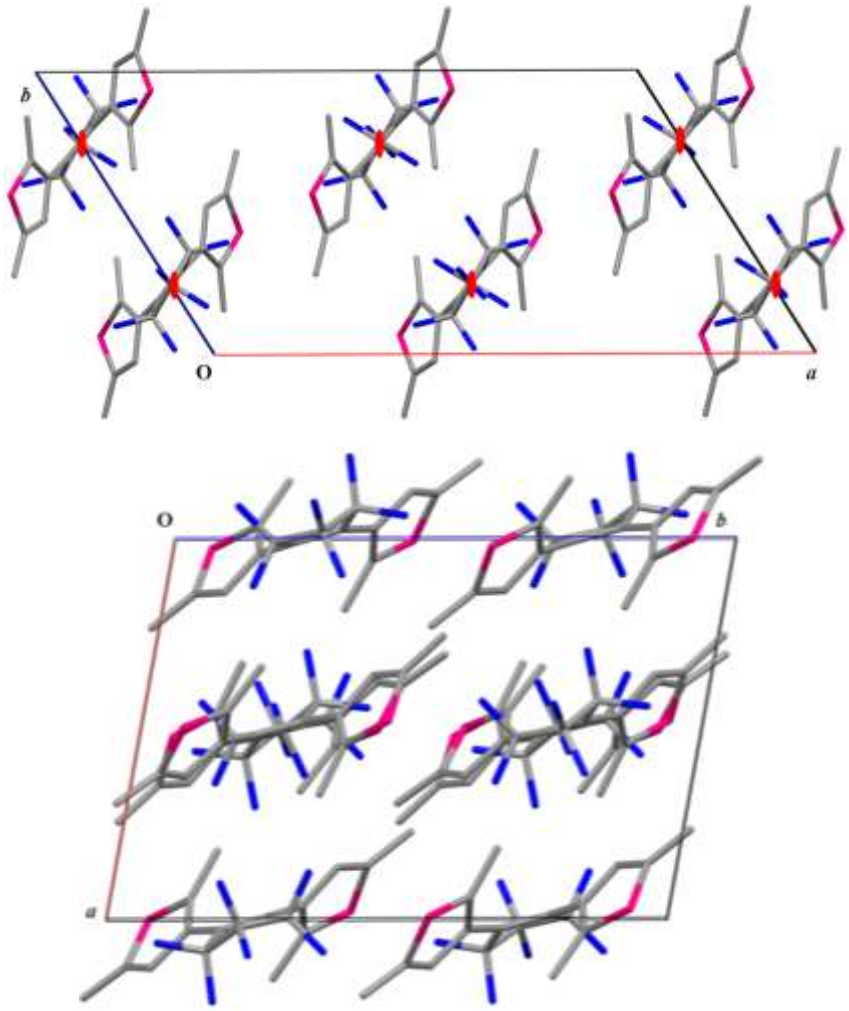

Figure 3. *C2/c* phase (Form-I) observed down the *c* axis. Red ellipses indicate the presence of a 2-fold rotation axis down the *b* axis Bottom) $P2_1/c$ phase (Form-II) viewed down c axis, note the loss of 2-fold symmetry.

Comparison of the two phases suggests that the loss of symmetry is not due to single change but is in fact made of multiple small and subtle changes, occurring in the hexafluorocyclopentene (HFCP) ring in combination with conformational distortions of the thiophene rings. The asymmetric

unit of the new $P2_1/c$ phase is given below in **Figure 4** to demonstrate how the asymmetric unit of the structure has changed in the new phase.

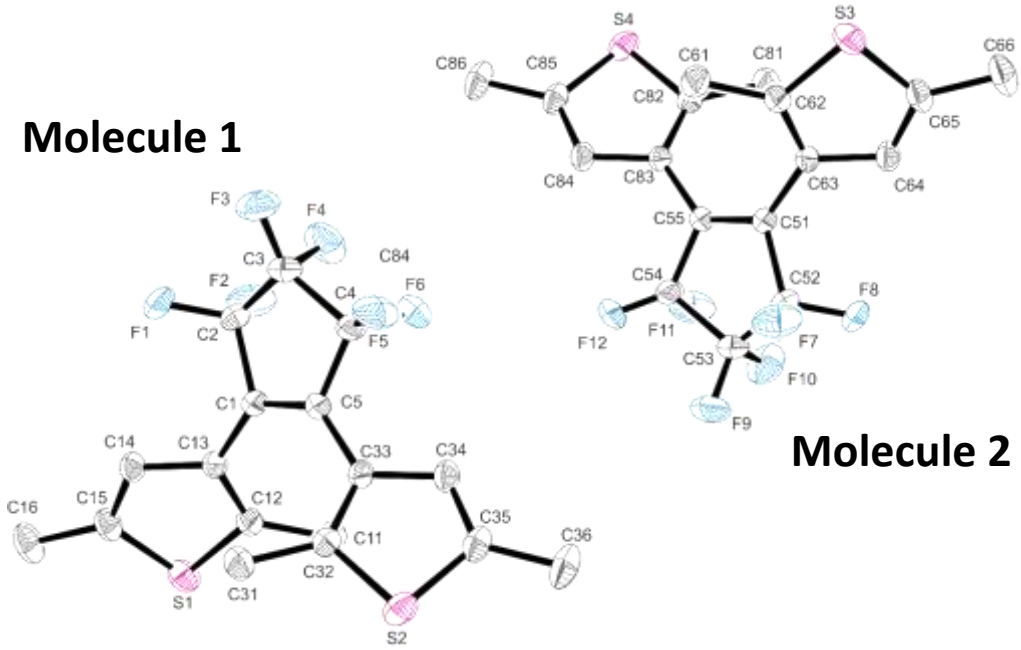

Figure 4. X-ray structure of 1 in the high pressure P21/c phase generated from the ambient structure.

As mentioned above there is significant distortion in the HFCP ring. Comparison of the HFCP ring before and after the phase transition shows that there is a puckering of the ring parallel to the direction of the *a* axis. Such behaviour can be expected to occur in situations involving low temperature or increased pressure, due to the reduced flexibility of the HFCP ring, in particular the C3 carbon and the fluorine atoms. These atoms tend to be highly disordered in the structures of DTEs due to flexibility of the HFCP ring but this problem can be overcome by data collection at lower temperature, resolving the group to a single position. It seems that in this case pressure seems to have a similar effect, restraining the flexibility of the HFCP ring to one position.

In Figure 5 the behaviour of the HFCP ring is examined more closely. While the structural distortion of the ring is quite clear by eye, indicated by the red arrows below, it is difficult to quantify the changes in terms of distances and angles altered due to the complex geometry of the ring.

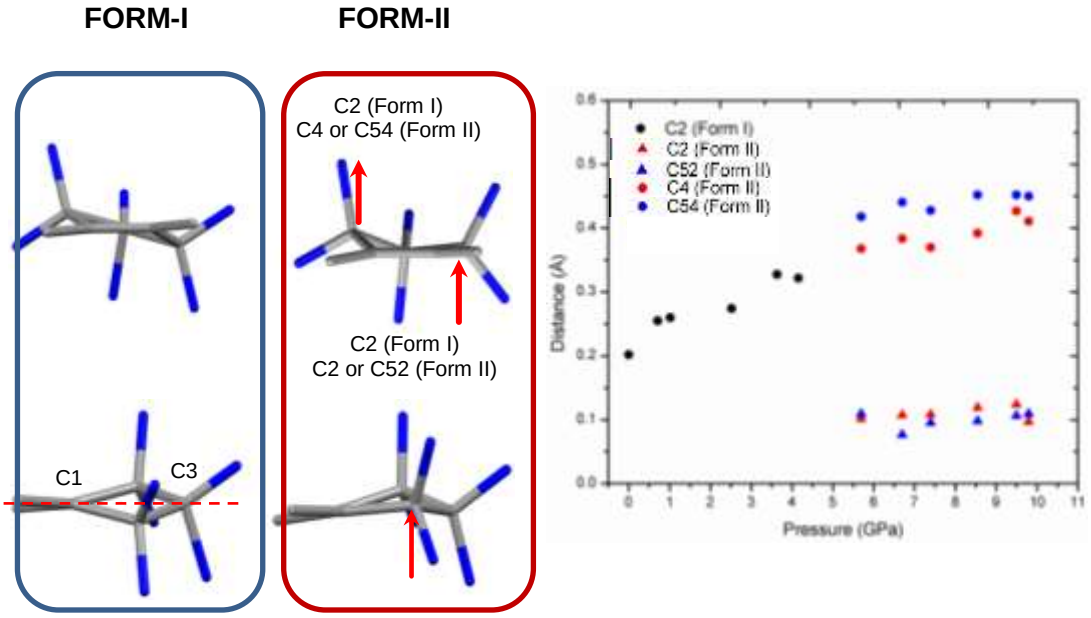

Figure 5. Left) HFCP ring in Form-I. Centre) HFCP ring in Form-II, with all other atoms omitted for clarity, red arrows indicate distortion. Right) Analysis of the displacement of noted atoms from a plane (C1-C3-C1 in Form-I;C1-C3-C4 and C51-C53-C54 of Form-II) in the HFCP ring in Form-I and Form-II.

If a plane is put through the C1 and C3 carbons in the Form-I structure, shown above and the equivalent atoms in Form-II, C1-C13-C5 and C51-C53-C55, it is possible to measure the distance by which the atoms move from the plane as the pressure is increased the values of which are given in graph above on the right.

We can see that before the phase change there is an upward trend, increasing the distance of the C2 carbon from the plane as pressure increases. However after the phase transition it appears that the four carbons in Form-II that replaced the one C2 carbon of Form-I behave differently from one another. From the graph above we can see that the C4 and C54 carbons continue the observed trend of increased distortion out of the plane. However it is clear the distortion is not mirrored across the other carbon as it was before the phase transition. There is a dramatic relaxation in distance from the plane in the C52 and C54 carbons which no longer continue to distort with increasing pressure.

These subtle variations reflect minor differences in the local environments of the carbon atoms in the rings concomitant with the lowering of the overall symmetry.

Other changes occur throughout the molecules as pressure is increased but these are more complex than the distortion of HFCP ring, involving the movement and rotation of many of the carbons relative to one another but continue the trend of asymmetric distortion within the system. The

figure below gives a visual representation of the distortion of the molecules in the structure of Form-II with increasing pressure, with the arrows displaying the trend in movement.

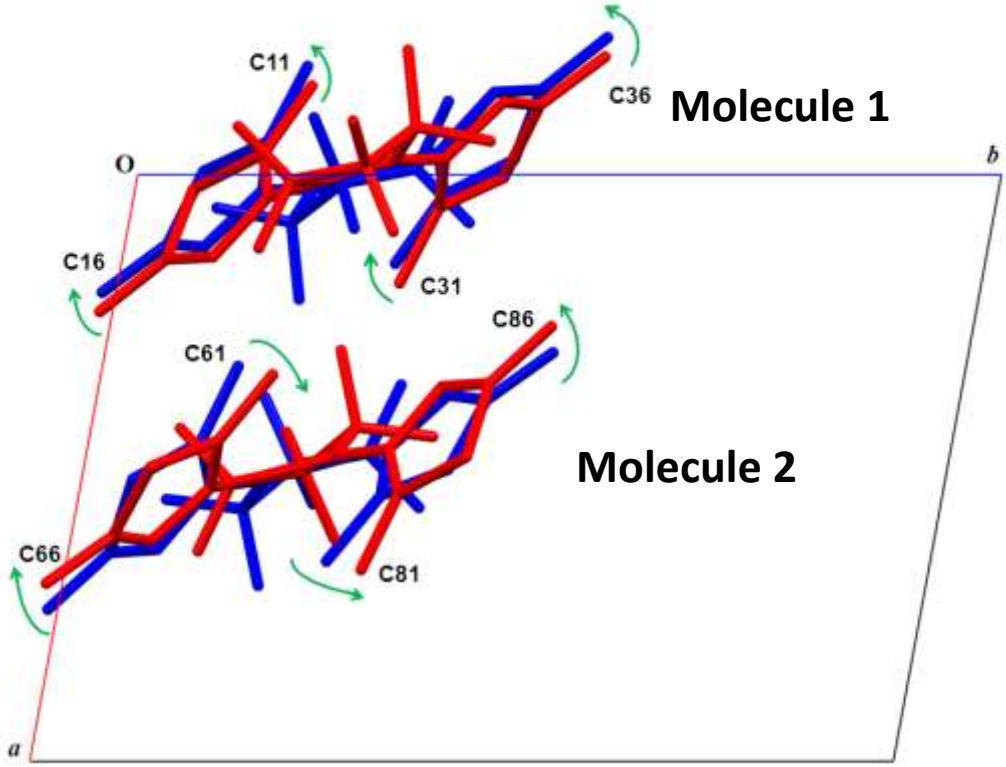

Figure 6. Distortion of molecules in Form-II relative to the plane displayed in Figure 7. Colour indicates molecules in the same asymmetric unit.

Once more the changes are easier to see visually than to quantify in terms of distances and angles. The easiest way to quantify the changes is to place a plane through the core atoms of the structure in a similar manner to that done earlier .Shown below is the plane against which the majority of molecular changes are measured running through four carbon atoms that make up the core of the molecule. In the *C2/c* phase the C13-C1-C1-C13 atoms and in the $P2_1/c$ phase the C13-C1-C5-C31 and the C63-C51-C55-C81are involved in the plane placement.

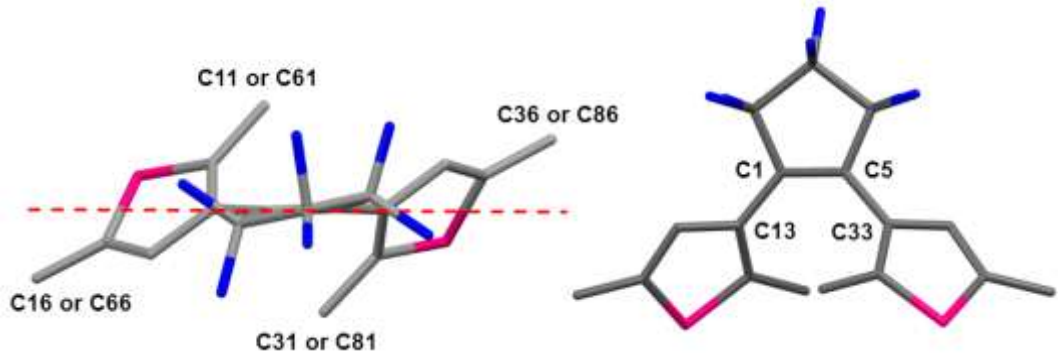

Figure 7. Left) Plane position through a molecule of **1** indicated by red dash. Right) Molecule of **1** with atoms selected for the plane labelled in one of the molecules of Form-I

It is interesting that two molecules in the asymmetric unit do not distort in identical ways. It is clear that the thiophene rings distort on both molecules relative to the HFCP ring of the molecule. The C11 and C16 carbons of the methyl groups on the thiophene provide a good way to characterise the

distortions that occur throughout the molecules as pressure increases by measuring the displacement of atoms relative to the planes placed through them.

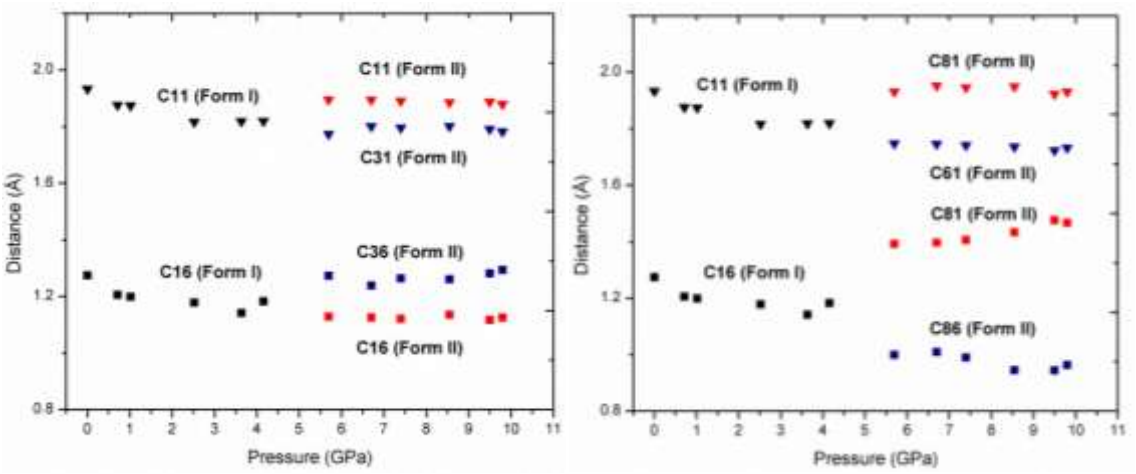

Figure 8. Left) Distance from plane to C11 and C16 atoms of form-I in black, Distances from equivalent atoms of molecule 1 in form-II in red and blue. Right) Distance from plane to C11 and C16 atoms of form-I in black, Distances from equivalent atoms of molecule 2 in form-II in red and blue.

In Form-I, shown in black in Figure 8, it is clear that there is only a small amount of movement in the C11 and C16 relative to the plane. The distance relative to plane is decreasing for both atoms suggesting that the rings are twisting slightly to lie more in the plane of the molecule.

After the phase transition there is a sudden change in some of the distances relative to the plane. In molecule 1 (C11, C16, C31, C36) the C11 atom jumps away from the plane while the C16 atoms continues to move closer. Similar behaviour is observed in the C31 and C36 carbons with C36 jumping away from the plane while C31 continues to move closer. Such behaviour suggests that perhaps the thiophene rings of molecule 1 are being distorted by both being pushed parallel to the *a* axis in a similar manner to the distortion of the carbons of the hexafluorocyclopentene ring discussed previously. Molecule 2 sees movement of the C61, C66, C81 and C86 atoms. C61 continues to move closer to the plane while C66 moves further away suggesting that the ring is twisting in a clockwise manner if viewed down the *b* axis. Interestingly it appears that the C81 and C86 move in a similar manner but anticlockwise therefore moving the thiophene ring so that it is becoming more perpendicular to the plane as opposed to parallel as seen with C61 and C66.

It is also interesting that the C12-C32, C62-C82 continue to move closer as the pressure is increased as shown in Figure 9. These carbons are interesting as they are important in terms of photochromism of the molecule and it has been suggested previously that their reactivity in the solid state is dependent on the distance between them.

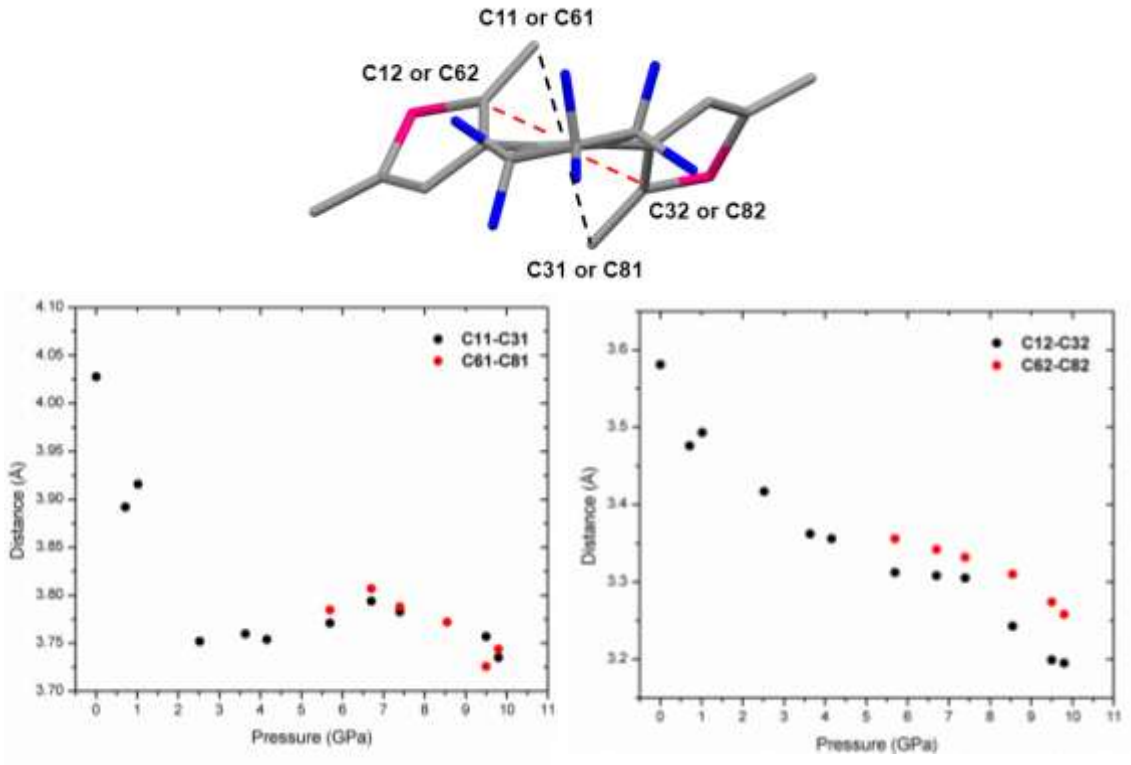

Figure 9. Top) Molecule of 1with the distances between the measured atoms labelled and marked. Bottom) Distances between selected carbon atoms

Structural Analysis of 1,2-Bis(2-methyl benzothiophen-3-yl)perfluorocyclopentene using the CLP program suite

The PIXEL method has previously been shown to be effective at quantifying the various interactions that occur within a crystal.[2] It has also been demonstrated to be useful at gaining a better understanding of phase transitions and intermolecular changes that can occur in a crystal at elevated pressures.[3-10] The PIXEL method is particularly useful as it enables the intermolecular forces present within a crystal structure to be broken down into their individual interactions and the energies involved down into coulombic, polarisation, dispersion and repulsion components.

As the pressure is increased, the overall lattice energy of the system increases (Figure 10). The lattice energy can be broken down and shows that the increase in lattice energy is largely due to the increasing value of the repulsive component of total energy. Interesting there appears to be no significant reduction in the packing energy between 4.45 GPa and 5.37 GPa as one might expect if a more energy favourable packing arrangement had been achieved.

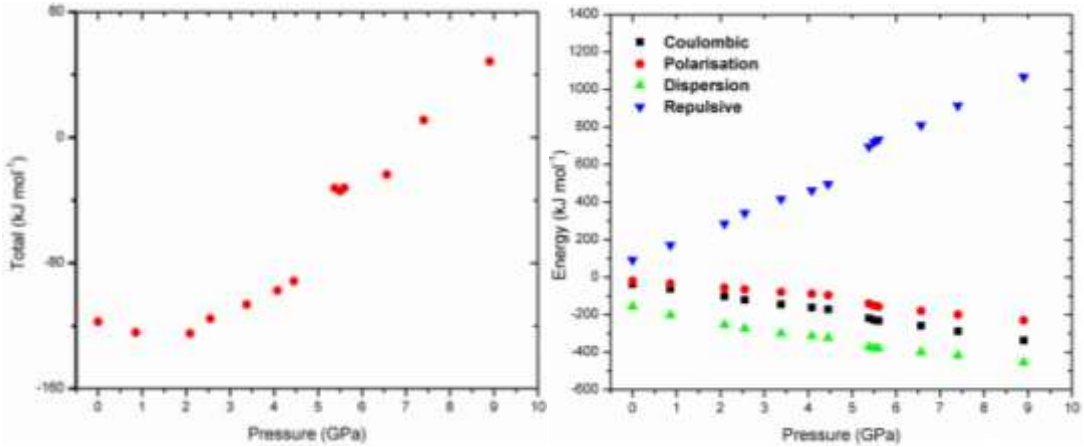

Figure 10. Total lattice energy as calculated by the Pixel method of the CLP programme suite Right) Combined coulombic (black), polarisation (red), dispersion (green) and repulsive energies generated by the Pixel program of the CLP program suite.

The PIXEL method only accounts for intermolecular interactions within the crystal lattice and does not take into account the large conformational changes that have occurred within the individual molecules. Such changes must be taken into account to gain a realistic estimate of the total lattice energy. No further calculations are required as GAUSSIAN 09 calculates the total molecular energy when creating the electron density map for the PIXEL calculation. Therefore the adjusted total lattice enthalpy (U_{adj}) can be calculated by subtracting the energy difference due to conformational change relative to the ambient structure from the PIXEL calculated total lattice energy, the results of which are given below in Table 5.

Table 5 Total Pixel lattice energy (E_{tot}) and their coulombic (E_{col}), polarisation (E_{pol}), dispersion (E_{disp}) and repulsion (E_{rep}) with pressure, Total lattice adjusted for changes in conformational structure (E_{adj}) and enthalpy at pressure (H).

GPa	Energy (kJmol^{-1})						
Pressure	**E_{col}**	**E_{pol}**	**E_{disp}**	**E_{rep}**	**E_{tot}**	**U_{adj}**†	**H**‡
0.00	-37.1	-17.8	-155.3	+92.9	-117.3	-117.3	-117.3
0.86	-61.6	-32.8	-201.8	+172.0	-124.3	-110.8	+138.3
2.09	-102.3	-55.4	-252.5	+285.4	-124.9	-106.1	+461.5
2.55	-120.4	-65.1	-272.9	+343.0	-115.4	-94.5	+581.3
3.38	-145.4	-79.3	-298.5	+417.0	-106.3	-82.6	+786.6
4.08	-160.4	-87.6	-312.4	+462.9	-97.5	-71.8	+961.9
4.45	-170.9	-94.8	-323.1	+497.3	-91.5	-62.5	+1053. 0
5.38	-218.3	-139.2	-372.1	+697.5	-32.2	+24.0	+1306.8
5.50	-228.5	-150.7	-377.3	+722.2	-34.2	+27.9	+1332.4
5.60	-232.2	-156.1	-378.4	+734.5	-32.1	+33.8	+1360.2
6.56	-258.1	-178.5	-399.1	+812.1	-23.6	+40.2	+1566.5
7.40	-287.1	-199.2	-417.2	+914.7	+11.3	+84.7	+1775.8
8.90	-336.5	-229.4	-454.7	+1069.1	+48.5	+132.1	+2108.0

† $U_{adj} = E_{tot}$ – (energy difference between molecular energy at pressure and molecular energy under ambient conditions as generated by GAUSSIAN 09 using the MP2/6-31G** basis set)

‡ Enthalpy (H) = U_{adj} + PV where P = pressure in Pascals (Pa) and V = molecular volume (m^3 mol^{-1})

It is clear from the calculations that the conformational changes within the crystal structure do not have a stabilising or negative energetic effect on the total lattice energy. An increase in lattice energy between Form-I and II of approximately +86 kJmol^{-1} (62.5+24.0) is observed but 56 kJmol^{-1} of this is due to the large conformational changes suggesting that both the changes in crystal packing and conformation result in a less energetically favourable phase in Form-II. Using the values of (U_{adj}) the values of enthalpy (H‡) can been calculated using the equation H = (U_{adj}) + PV where P = pressure (Pa) and V = molar volume (mol m^{-3}) the results of which are also given in Table 5. The lattice enthalpy becomes increasing positive, dominated by the PV term. The enthalpy for the two phases may be examined individually using linear lines of best fit.

Figure 11 displays a line of fit fitted to Form-I where the line is extrapolated to higher pressures. It is clear from the graph that all the data points of Form-II sit on or below the line of as pressure increases above 5.38 GPa. There does not appear to be a dramatic discontinuity between the two phases as has been reported in other systems. If the experimentally obtained value of H‡ is compared to that estimated from the line of fit at 5.38 GPa, the lowest Form-II data point, a -0.4 kJmol^{-1} discrepancy is observed however there is a definite change in gradient of the lines as shown clearly on the right of Figure 11 something that is consistent with other high pressure induced transitions of this sort.[11] At the highest pressure observed of 8.90 GPa, the discrepancy has reached the value of -111.69 kJmol^{-1} suggesting that Form-II is significantly more stable at higher pressures than Form-I, indicating the formation of a more thermodynamically stable phase at high pressure.

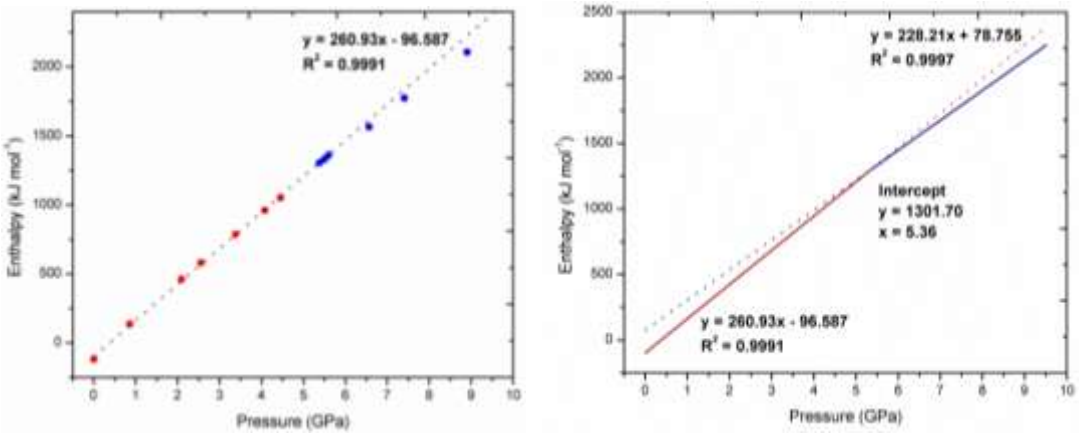

Figure 11. Left) Lattice enthalpy of **2** with pressure. A linear line of best fit has been plotted and extrapolated to higher pressure. Right) Linear lines of fit for both phases with the point of intercept displayed.

Pixel analysis of individual interactions

The Pixel method works out the total energies involved within a crystal structure by summing all individual interactions present with a crystal. Therefore, it is possible to analyse how all the individual interactions behave within a crystal as it is pressurised. Pixel analysis of the eight most significant interactions within the structures provides interesting detail into how pressure affects the intermolecular forces present within the crystal.

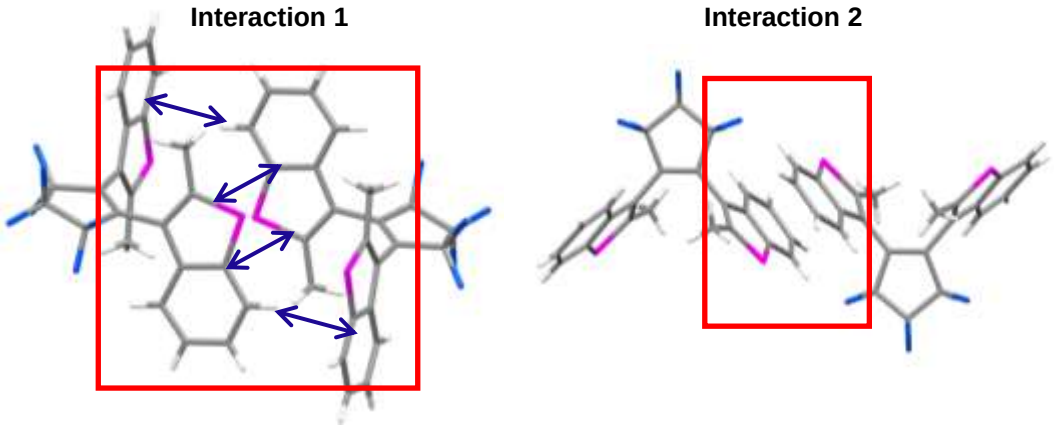

Figure 12. The two most significant interactions present in the unit cell of **2** as generated by pixel, blue arrows indicate reduction with pressure. Symmetry operators: (1) 1-x,-y,1-z; (2) 2-x,-y,2-z .

The two strongest interactions as determined by the PIXEL method are given above in Figure 12. Within the crystal structure of **1** there is an absence of defined and hard intermolecular interactions such as hydrogen bonds around which conventional crystal analysis is based. However the Pixel method does well to quantify the softer and more complex interactions present in the structure. Interaction 1 of Figure 12 appears to be a combination of a π…π stacking interaction between symmetry related benzothiophene rings, C-H…π interactions between the C-H of the

benzothiophene rings and the opposing ring, as well as a CH_3 interaction with the opposing ring. Interaction 2 is less complex being a π…π interaction between two benzothiophene rings with the distance between them compressing with pressure. Both terms are dominated by the dispersive component of their interactions at low pressures with some evidence suggesting that the total energy of the interactions becomes more negative i.e. stabilising at lower pressures, however as pressure increases the repulsive term increases to dominate the energies of the interactions as shown in Figure 13.

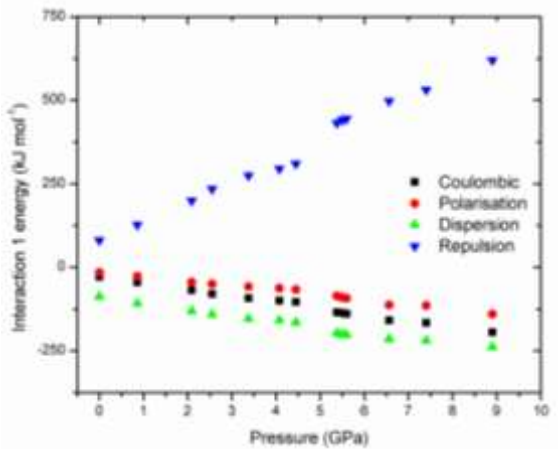

Figure 13. Combined coulombic (black), polarisation (red), dispersion (green) and repulsive (blue) energies generated by the PIXEL program of the CLP program suite for interaction 1

Table 6 The 8 most significant interaction contained in the unit cell of (2) in terms of contribution to total lattice energy and their variation with pressure as calculated by the pixel module of the CLP program suite.

GPa	Energy ($kJmol^{-1}$)							
Pressure	**1**	**2**	**3**	**4**	**5**	**6**	**7**	**8**
0.00	-50.7	-32.3	-24.1	-17.6	-17.4	-12.0	-7.3	-4.8
0.86	-51.7	-32.5	-24.9	-18.0	-19.0	-13.3	-5.3	-8.0
2.09	-42.9	-35.1	-26.2	-17.2	-20.9	-13.7	-5.1	-8.2
2.55	-34.9	-27.2	-24.9	-15.3	-21.3	-13.6	-4.8	-8.3
3.38	-29.9	-24.5	-24.8	-13.2	-19.9	-12.8	-4.0	-7.4
4.08	-25.6	-23.0	-23.5	-11.2	-18.6	-11.4	-3.6	-6.4
4.45	-23.8	-21.9	-22.7	-10.6	-16.9	-10.1	-3.3	-5.7
5.38	+14.8	+14.2	-26.5	-9.8	+0.8	+4.8	-9.1	-9.8
5.50	+12.2	+5.9	-25.2	-7.9	+1.6	+5.2	-9.2	-10.5
5.60	+11.4	+8.3	-24.7	-7.8	+1.8	+6.1	-9.1	-10.3
6.56	+12.2	+12.7	-26.0	-4.6	+3.3	+8.3	-8.6	-10.3
7.40	+33.3	+23.4	-16.8	+0.8	+7.5	+11.8	-6.7	-10.1
8.90	+46.4	+49.8	-16.3	+8.1	+12.7	+15.0	-4.6	-9.6

Interactions 3-8 are all significantly less energetic than 1 and 2, as shown in table 6 and appear to be based upon C-F…H or weaker C-H…π interactions as shown in Figure 14. The majority of the interactions behave in a similar manner to that of 1 and 2 with the dispersive element of their interaction dominating the lower pressures but becoming increasingly destabilising as the repulsive term begins to dominate at higher pressures

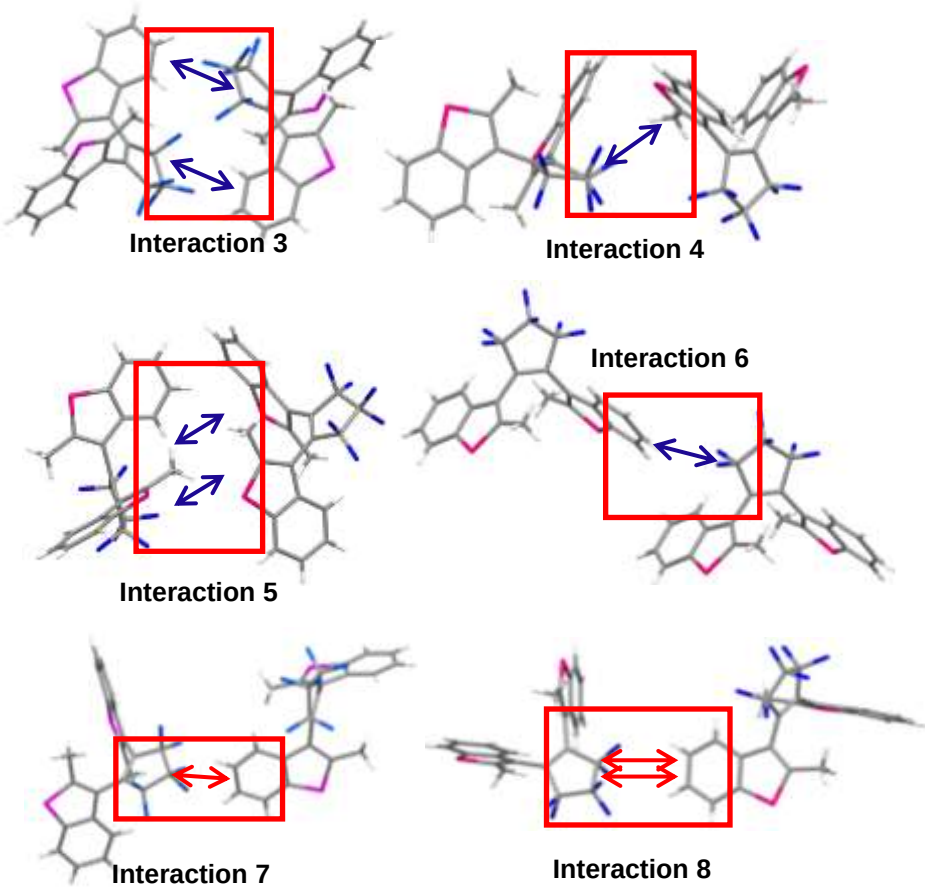

Figure 14. Six more significant interactions present in the unit cell of **2** as generated by pixel, blue arrows indicate reduction with pressure, red arrows indicate expansion. Symmetry operators: (3) 1-x,-y,2-z; (4)1/2+x, 1/2 -y, 1/2+z; (5) 3/2-x,1/2+y,3/2-z; (6) x,y,-1+z; (7) 1/2+x, 1/2-y,z-1/2; (8) 1/2-x, 1/2+y,3/2-z

Interaction 5 is unique among the interactions as it is the only interaction where the polarisation component of the interaction becomes more dominant relative to the other terms with the exception of the repulsive as shown in the top of Figure 15. It is interesting that the during the phase transition the coulombic and polarisation interaction become more negative than expected but the dispersive interaction jumps to becoming less stabilising in a similar manner to the repulsive term.

Interactions 7 and 8 are the smallest interactions in terms of energy but they are interesting as they are the only interactions that become more stabilising upon the phase transition as shown for interaction 8 in Figure 15. When the nature of these interactions is examined it is clear that such a reduction is due to the hydrogens of the benzothiophene ring moving away from the fluorines of the HFCP ring on the opposing molecule as shown at the bottom of Figure 14.

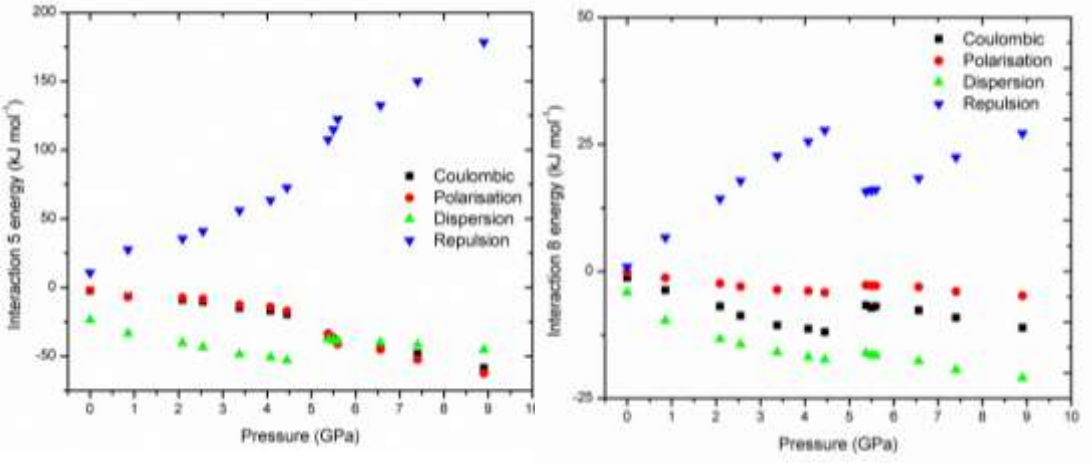

Figure 15. **.** Breakdown of interaction of 5 and 8 into coulombic, polarisation, dispersion and repulsion components.

Spectroscopic details

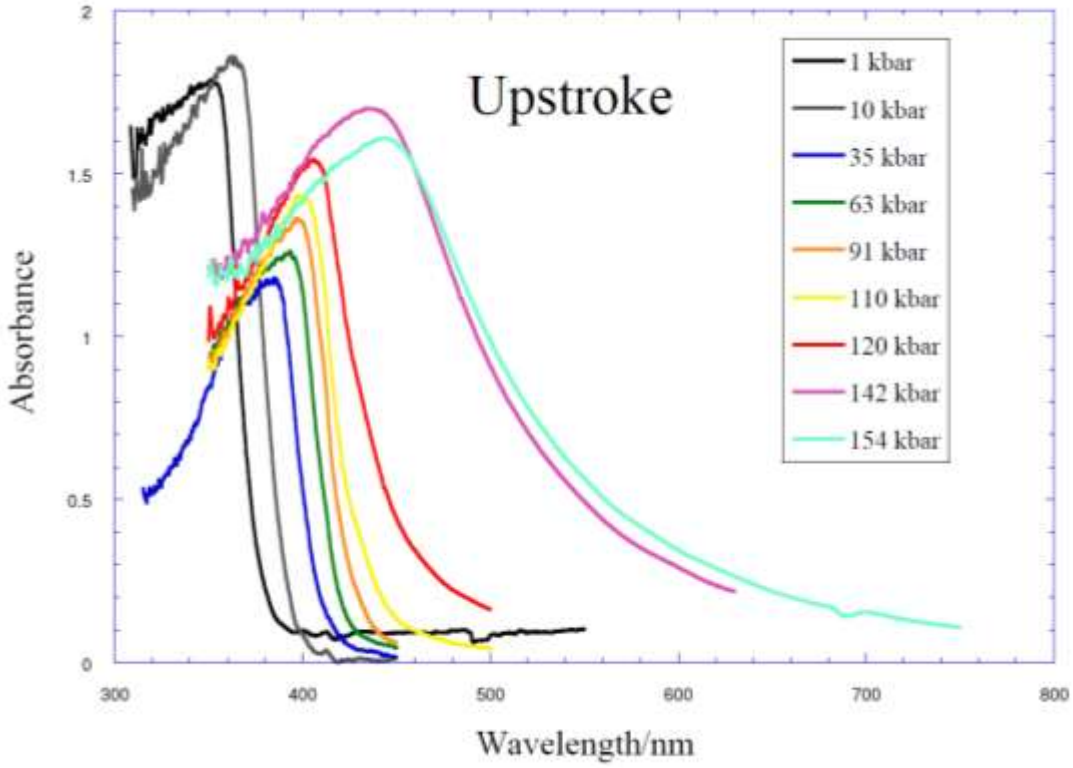

Figure 16. High pressure UV-Vis spectra of **1** collected upon increasing pressure

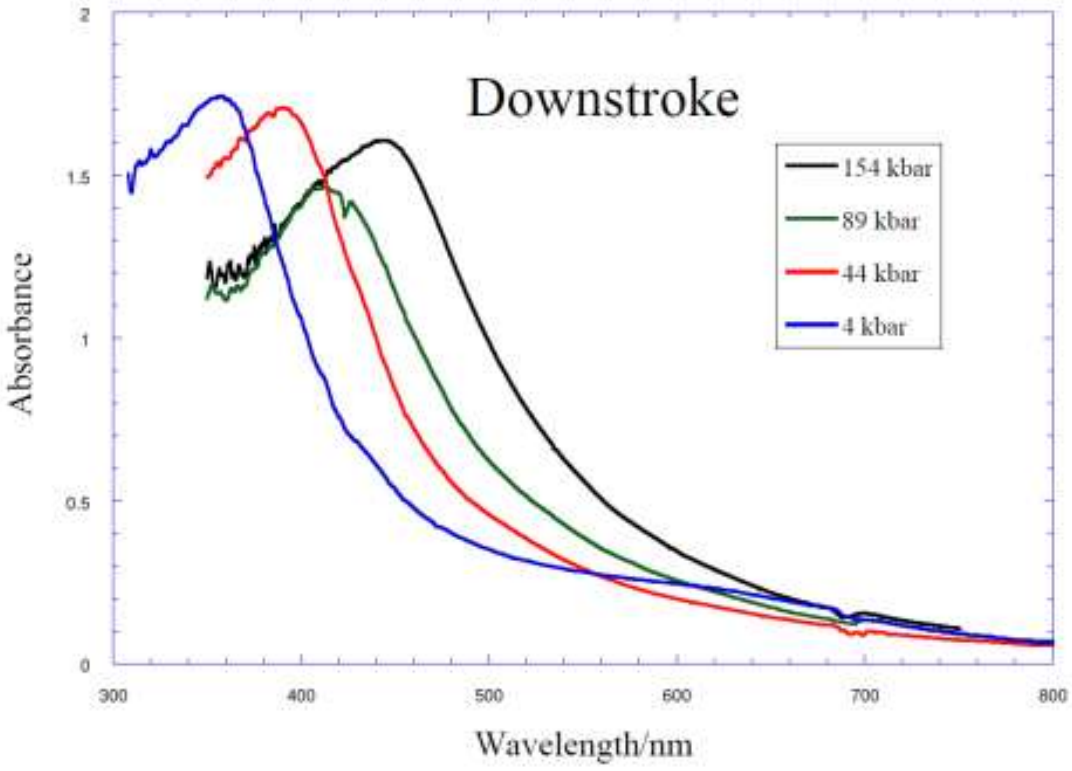

Figure 17. High pressure UV-Vis spectra of **1** collected upon decreasing pressure

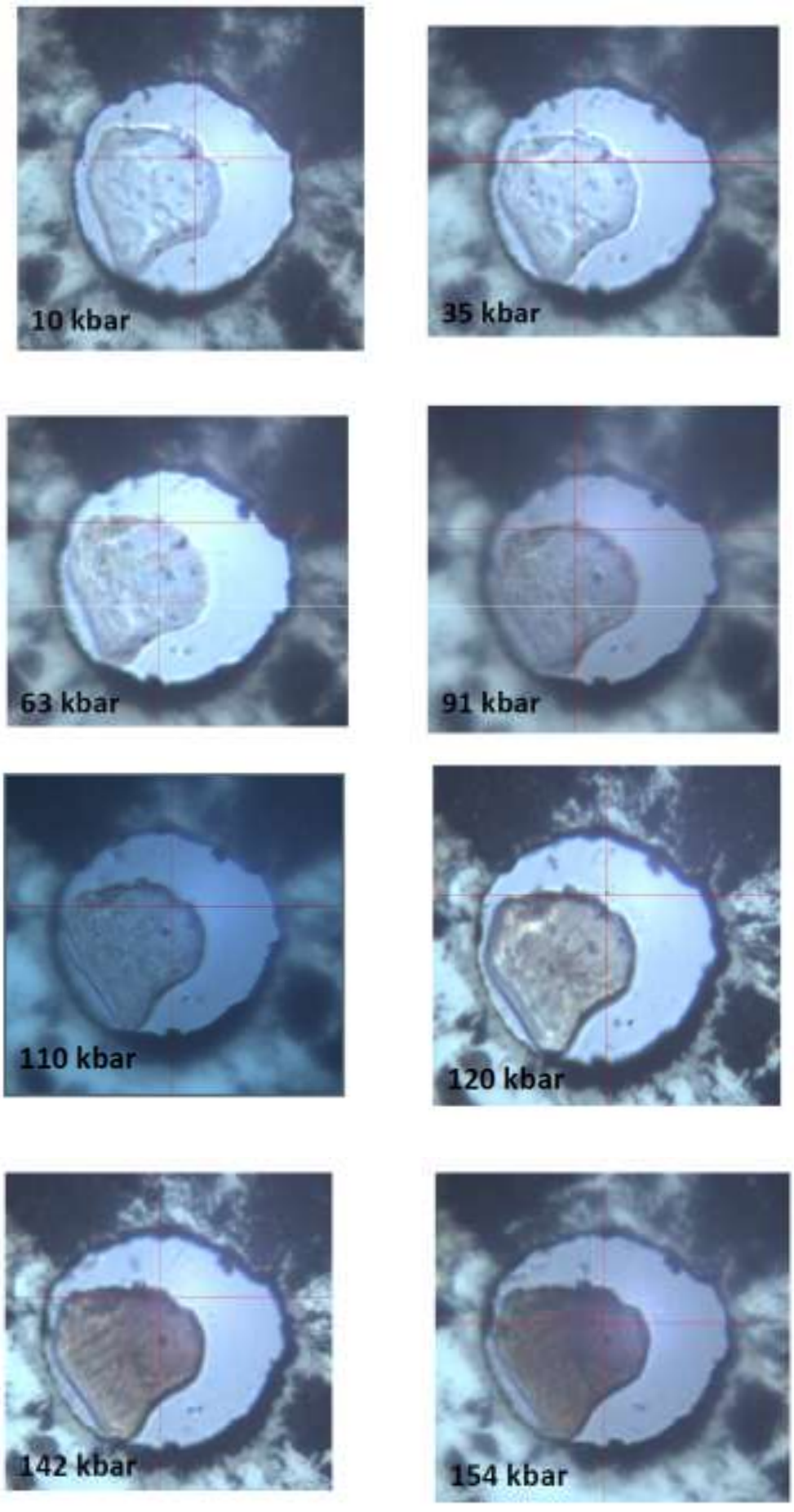

Figure 18. Photograph of **1** at varying pressures

1. **R. Angel, *EOSFIT version 5.2*, (2002).**
2. **K. Durka, A. A. Hoser, R. Kaminski, S. Lulinski, J. Serwatowski, W. Kozminski and K. Wozniak, *Cryst. Growth Des.*, 2011, 11, 1835-1845.**
3. **S. A. Moggach, S. Parsons and P. A. Wood, *Crystallography Reviews*, 2008, 14, 143-183.**
4. **P. A. Wood, J. J. McKinnon, S. Parsons, E. Pidcock and M. A. Spackman, *CrystEngComm*, 2008, 10, 368-376.**
5. **R. D. L. Johnstone, A. R. Lennie, S. F. Parker, S. Parsons, E. Pidcock, P. R. Richardson, J. E. Warren and P. A. Wood, *CrystEngComm*, 2010, 12, 1065-1078.**
6. **N. P. Funnell, A. Dawson, D. Francis, A. R. Lennie, W. G. Marshall, S. A. Moggach, J. E. Warren and S. Parsons, *CrystEngComm*, 2010, 12, 2573-2583.**
7. **N. P. Funnell, A. Dawson, W. G. Marshall and S. Parsons, *CrystEngComm*, 2013, 15, 1047-1060.**
8. **P. A. Wood, D. Francis, W. G. Marshall, S. A. Moggach, S. Parsons, E. Pidcock and A. L. Rohl, *CrystEngComm*, 2008, 10, 1154-1166.**
9. **P. A. Wood, R. S. Forgan, D. Henderson, S. Parsons, E. Pidcock, P. A. Tasker and J. E. Warren, *Acta Crystallogr. Sect. B-Struct. Sci.*, 2006, 62, 1099-1111.**
10. **R. D. L. Johnstone, D. Francis, A. R. Lennie, W. G. Marshall, S. A. Moggach, S. Parsons, E. Pidcock and J. E. Warren, *CrystEngComm*, 2008, 10, 1758-1769.**
11. **N. V. C. Shekar and K. G. Rajan, *Bull. Mater. Sci.*, 2001, 24, 1-21.**